PCCP

COMMUNICATION

View Article Online
View Journal | View Issue



Cite this: *Phys. Chem. Chem. Phys.*, 2015, **17**, 22561

Received 10th April 2015,
Accepted 30th July 2015

DOI: 10.1039/c5cp02103k

www.rsc.org/pccp

# Exploration of minimum energy conical intersection structures of small polycyclic aromatic hydrocarbons: toward an understanding of the size dependence of fluorescence quantum yields†

Yu Harabuchi,[ab] Tetsuya Taketsugu[ab] and Satoshi Maeda*[ab]

**Minimum energy conical intersection (MECI) geometries were searched for polycyclic aromatic hydrocarbons (PAHs) consisting of up to 26 atoms. The energy barriers to the obtained MECIs showed a correlation with their fluorescence quantum yields. This provides a theoretical rationale for the size dependence of the fluorescence quantum yields seen in these PAHs.**

## Introduction

The importance of the conical intersection (CI) in photochemical reactions has been noted in a number of studies.[1–6] With particular regard to the ultrafast photo-decay process, several observations have been made of dynamics of species undergoing a nonadiabatic transition near the CI region.[7–10] If a stable CI region that a molecule can access easily from the Franck–Condon (FC) region is present, an ultrafast non-radiative decay occurs dominantly upon photo-absorption. In this case, *ab initio* molecular dynamics (AIMD) simulations are ideally suited to an examination of the non-statistical dynamics of the ultrafast photoreaction. Such short-timescale (sub-10–100 picoseconds) AIMD simulations have been made possible by increases in computing power.

The CI region also plays a role in *non*-ultrafast photoreactions. For example, fluorescent molecules stay on the electronic excited-state potential energy surface (PES) on sub-nano- to micro-second timescales. In this case, radiative and non-radiative decays compete with each other, and their competition determines the fluorescence quantum yield. When the energy barriers to reach CI regions are sufficiently high, and are thus difficult to access from the FC region, the fluorescence process is dominant. However, AIMD simulations of the electronic excited-state PES on sub-nano- to micro-second timescales remain highly demanding, even for small molecules. Thus, in this study, we tackled the problem by directly finding minimum energy conical intersections (MECIs).

The MECI is the lowest energy point within a CI hyperspace, and MECI geometries have been optimized as a critical point, or a representative geometry, of the nonadiabatic transition.[11–18] However, preparing initial geometries for MECI optimizations is not trivial, because MECI geometries are generally distant from the stable geometries in the ground state. Motivated by this, the seam model function (SMF) approach was proposed to find the all-important MECIs.[19] In the SMF, automated stable structure search methods are initially applied to a model function on which approximate MECI structures can be obtained as local minima. These approximate structures are then optimized using a standard MECI optimization technique. This approach has been used extensively in the studies of the photodissociation mechanisms of small molecules.[20] Recently, its applicability has been improved dramatically by the use of the spin–flip time dependent density functional theory (SF-TDDFT)[21–23] in the electronic structure calculations and the use of the single-component artificial force induced reaction (SC-AFIR)[24] method in the automated stable structure search.[25,26]

In the present study, MECI geometries for the lowest two singlet electronic states (denoted $S_1/S_0$-MECI) were systematically searched using the SMF/SC-AFIR/SF-TDDFT approach. These searches were applied to the five polycyclic aromatic hydrocarbons (PAHs) shown in Fig. 1 and initiated from their FC points. Transition state (TS) geometries between the FC region and the obtained MECIs were also determined. Based on the energies of the obtained MECI and TS structures, the size dependence of the fluorescence quantum yields seen in these PAHs is discussed.

## Target system

In this study, the five smallest PAHs (listed in Fig. 1) were considered. The ground state electronic structures[27–31] and

[a] *Department of Chemistry, Faculty of Science, Hokkaido University, Sapporo 060-0810, Japan. E-mail: smaeda@mail.sci.hokudai.ac.jp*
[b] *CREST, Japan Science and Technology Agency, Tokyo 102-8666, Japan*

† Electronic supplementary information (ESI) available: All of the MECI geometries and the relative energies are shown. See DOI: 10.1039/c5cp02103k

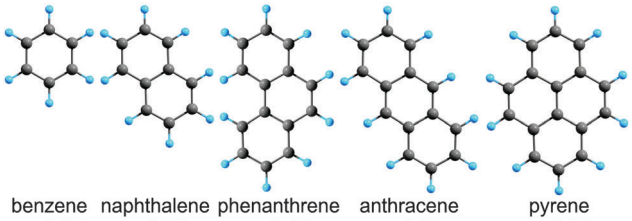


Fig. 1 Molecular geometries of five PAHs: benzene, naphthalene, phenanthrene, anthracene, and pyrene. The experimental fluorescence quantum yields (measured in cyclohexane) are also shown for each molecule.[34]

vertical excitation energies of these molecules have been studied extensively.[32,33] The larger of these five PAHs exhibit larger fluorescence quantum yields, as summarized in Fig. 1.[34] There are two possible reasons for this: (1) the radiative decay is faster in the larger PAHs, and/or (2) the non-radiative decay is slower in the larger PAHs. To discuss the latter, it is necessary to identify important non-radiative decay channels. In particular, the energy barrier to reach one of the $S_1/S_0$-MECIs indicates how often the molecule can reach a region with a small $S_1$–$S_0$ energy gap. Thus, locating all of the stable $S_1/S_0$-MECIs provides a reasonable starting point for a discussion of the efficiency of the non-radiative decay.

The $S_1/S_0$-CI regions and the $S_1/S_0$-MECI structures of benzene have been studied thoroughly by Robb and co-workers.[35–37] However, the $S_1/S_0$-MECIs for the larger PAHs have not been studied in detail. In this study, we therefore systematically explored the MECIs of the larger PAHs using the SMF/SC-AFIR/SF-TDDFT approach, and we discuss here the efficiency of the non-radiative decay.

## Results and discussion

From the SMF/SC-AFIR/SF-TDDFT searches, 6, 12, 26, 14, and 17 independent MECI structures were found for benzene, naphthalene, phenanthrene, anthracene, and pyrene, respectively. Because of the lower symmetry in phenanthrene, the number of independent structures in phenanthrene was larger than that in the larger PAH, pyrene. The local minimum structures on the $S_1$ surface near the FC region ($S_{1\,MIN}$) were also optimized from each FC point, and the TS geometries between the $S_{1\,MIN}$ and the MECIs were then optimized. The connection of the $S_{1\,MIN}$ and the MECIs through the TSs was finally confirmed by the intrinsic reaction coordinate (IRC) calculations. The $S_{1\,MIN}$ geometries, the TS geometries, the MECI geometries, and their relative energies are shown in the ESI.†

The $S_{1\,MIN}$, the three most stable MECIs, and the related TSs for each PAH are summarized in Fig. 2. A low-energy MECI with a CH bond dissociation for pyrene was excluded, because a high-energy TS providing a route to the CI region was found. The most stable MECI geometry for benzene (shown in Fig. 2) was consistent with that determined in previous studies.[35–37] The FC point and the three most stable MECIs for benzene were further optimized using the CASPT2/cc-pVDZ method. The $S_1$ energies determined using the CASPT2 method for the optimized FC, MECI1, MECI2 and MECI3 geometries of benzene were 4.84 eV, 4.97 eV, 5.07 eV, and 5.17 eV, respectively, relative to the ground state benzene. The geometries and the order of the relative energies were consistent with the SF-BHHLYP results shown in Fig. 2 (see the ESI† for the geometries).

As shown in Fig. 2, the $S_{1\,MIN}$ geometries were planar for all of the PAHs. In Fig. 2, the label "N/A" for the $S_{1\,MIN}$ of phenanthrene indicates that the corresponding local minimum was not found. That is, the optimizers implemented in both GRRM and GAMESS showed oscillating behavior, and ultimately failed to reach a converged geometry. This oscillation was caused by the instability of the SF-TDDFT calculations for geometries in which the reference triplet state was nearly degenerate with the other triplet state. Although most of the MECIs were accessed from the $S_{1\,MIN}$ in one step *via* a single TS, there were two cases showing two barriers, and one case in which there was no barrier. The MECI2 of benzene and the MECI3 of naphthalene fell into the two-barrier classification; for these two, only the higher TS is shown in Fig. 2. In the two-step path to the MECI2 of benzene, MECI3 was the intermediate, and MECI2 and MECI3 were connected by a small barrier. Among the two TSs along this path, the first TS between $S_{1\,MIN}$ and MECI3 was higher than the second TS between MECI3 and MECI2. Thus, in Fig. 2, the first TS, which was identical to TS2, is presented as TS3. Similarly, for the MECI3 of naphthalene, $S_{1\,MIN}$ and MECI3 were connected by two steps *via* the fourth stable MECI (see MECI4 in the ESI†). The TS connecting $S_{1\,MIN}$ and MECI4 was higher than that between MECI4 and MECI3, and the former TS is shown as TS3 in Fig. 2. The MECI3 of anthracene corresponded to the case with no barrier; the corresponding TS3 is indicated by "N/A" in Fig. 2. This was confirmed by the meta-IRC (the mass-weighted steepest descent path) determined from the MECI3 of anthracene; the meta-IRC led directly to $S_{1\,MIN}$.

From the extensive list of MECI structures shown here, it was found that the stable MECI geometries for the PAHs could be categorized into three types characterized by the three stable MECI structures determined for benzene. In other words, the structural deformations in the stable MECIs were localized on a single ring in these small PAHs. Consequently, the relative energies for the most stable MECIs fell within a narrow range of 4.94–5.57 eV, as shown in Fig. 2.

Here, we discuss the magnitude of the fluorescence quantum yields based on the shape of potential energy surfaces. Fig. 3A and B show schematic illustrations of two different potential profiles: one illustrates the case in which the non-radiative decay is dominant (Fig. 3A), and the other illustrates the case in which the radiative decay with fluorescence is dominant (Fig. 3B). Fig. 3A shows an MECI in a lower energy region, relative to the FC point; in this case a non-radiative, ultrafast decay *via* the related CI region can take place. In the case of Fig. 3B, the lowest energy MECI is much higher in energy than the FC point. Hence, the access frequency of a molecule to the CI region is low, and the non-radiative decay should thus be slow. In other words, the relative importance of the radiative decay is high. In this manner, one can discuss the relative importance of the radiative

 

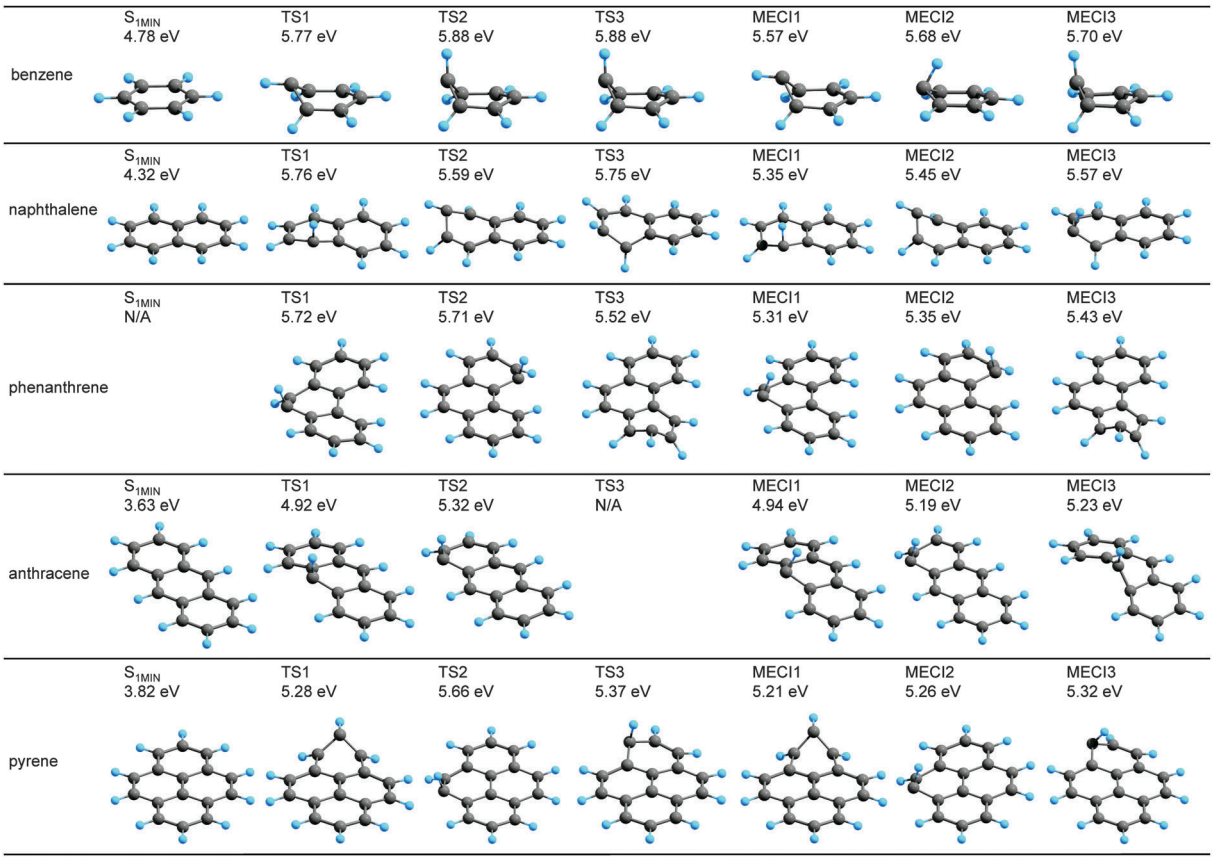


Fig. 2 $S_1$-minimum geometries near the FC point ($S_{1\,MIN}$), the three most stable MECI geometries, and the TS geometries to reach the lowest three MECIs from $S_{1\,MIN}$ for the five PAHs benzene, naphthalene, phenanthrene, anthracene, and pyrene. All the geometries were optimized using SF-BHHLYP/6-31G*. For each system, the potential energy of each geometry is given relative to the $S_0$ energy in the ground state equilibrium structure. All the obtained geometries are summarized in the ESI.† The $S_{1\,MIN}$ of phenanthrene could not be optimized at SF-BHHLYP, and the TS3 of anthracene did not exist, so these entities are shown as "N/A".

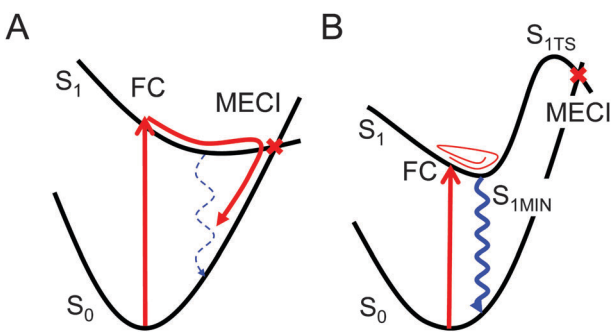


Fig. 3 Schematic illustration of the potential energy surfaces for two types of photo-reactions. (A) The case in which the ultrafast non-radiative decay *via* a CI region (see the red arrow) is dominant. (B) The case in which the decay *via* a fluorescence process (highlighted by the waved blue arrow) is dominant.

decay by comparing the energy difference between the most stable MECI and the FC point, *i.e.*, $E_{\text{Lowest–MECI}} - E_{\text{FC}}$. For a more quantitative prediction, the $S_{1\,MIN}$ and the TS connecting the $S_{1\,MIN}$ and the CI region are required, as illustrated in Fig. 3B. Based on the transition state theory,[38] the Gibbs free energy gap between the $S_{1\,MIN}$ and the TS, *i.e.* $G_{S1\,TS} - G_{S1\,MIN}$, can be compared directly with the access frequency of a molecule to the CI region. In this study, the $E_{\text{Lowest–MECI}} - E_{\text{FC}}$ and $G_{S1\,TS} - G_{S1\,MIN}$ gaps were compared with the experimental fluorescence quantum yields, where $G_{S1\,TS} - G_{S1\,MIN}$ corresponds to the Gibbs free-energy gap at 298.15 K and 1 atm.

With this information in mind, the experimental fluorescence quantum yields were plotted against the two calculated energy differences, *i.e.*, the $E_{\text{Lowest–MECI}} - E_{\text{FC}}$ gap and the $G_{S1\,TS} - G_{S1\,MIN}$ gap, for the five PAHs, as shown in Fig. 4. The $G_{S1\,TS} - G_{S1\,MIN}$ gap for phenanthrene was excluded from Fig. 4, because the $S_{1\,MIN}$ geometry was not found at the SF-BHHLYP level, as noted above. As expected, the $G_{S1\,TS} - G_{S1\,MIN}$ gap showed a clear correlation with the experimental fluorescence quantum yields. For these PAHs, the $E_{\text{Lowest–MECI}} - E_{\text{FC}}$ gap also correlated well with the fluorescence quantum yields. This was because the TSs were close to the MECIs, and the $S_{1\,MIN}$ were also close to the FC point. Thus, in the following, the origin of the size dependence of fluorescence quantum yields is discussed based on the nature of the FC point and the MECIs.

For these PAHs, $E_{\text{FC}}$ or the experimental excitation energy decreases with increase in the molecular size because of the strong stabilization of the $\pi$–$\pi^*$ states that results from the delocalization of the $\pi$ and $\pi^*$ orbitals. However, the

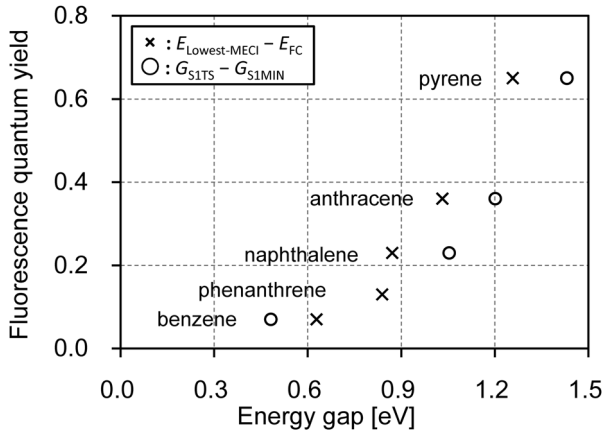


Fig. 4 Diagram illustrating the correlation between the fluorescence quantum yields measured in cyclohexane[34] and the two energy gaps, $E_{Lowest-MECI} - E_{FC}$ (cross marks) and $G_{S1\,TS} - G_{S1\,MIN}$ (circles). Each PAH is indicated with the name of the PAH.

observation that $E_{Lowest-MECI}$ did not differ very much for the different PAHs was new; this phenomenon occurred because the structural deformations in the stable MECIs were localized on a single ring, as shown in Fig. 2. Based on this result, we proposed that the delocalized and localized characters of the $S_1$ at the FC point, and the $S_1$ at the lowest MECI geometry, allowed the larger PAHs to emit stronger fluorescence for the PAHs studied here.

We note that in this study we did not consider a number of factors, including the rate of radiative decay, the contributions of the triplet states, and the weak vibronic coupling around the $S_1$ local minimum. A more quantitative analysis considering all of these factors together will be performed in a future study working toward the quantitative prediction of fluorescent quantum yields. Finally, we emphasize that the present approach is promising for illustrating the impact of the non-adiabatic transition near the CI in fluorescence quenching.

## Conclusion

In the present study, $S_0/S_1$-MECIs were searched systematically using our own automated MECI search method, SMF/SC-AFIR/SF-TDDFT. The search was applied to five PAHs—benzene, naphthalene, phenanthrene, anthracene, and pyrene—and a total of 6, 12, 26, 14, and 17 independent $S_0/S_1$-MECI geometries were obtained, respectively. It was found that structural deformations in the stable MECIs were localized on a single ring, and that all of the stable MECIs could be classified into three types that were reported previously for benzene. Because of the localized nature of the stable MECIs, their relative energy did not depend strongly on the PAH size. In contrast, the vertical excitation energy decreases with increase in the PAH size. As a consequence, the energy barrier between the FC point and the lowest CI point increased with increase in the PAH size.

Based on the extensive MECI structural database determined here, an interesting correlation between the fluorescence quantum yields and the energy barrier to the CI region was discovered for these five small PAHs. This suggested that two processes—specifically, radiative decay with the emission of fluorescence and nonradiative decay near the conical intersection—were in competition. This correlation provided a theoretical explanation for the observed experimental trend that the larger PAHs showed stronger fluorescence. Further applications of the present approach to other fluorescent systems are in progress to investigate the generality of this correlation.

## Computational details

The $S_0/S_1$-MECI geometries of five PAHs, benzene, naphthalene, phenanthrene, anthracene, and pyrene, were searched using the SMF/SC-AFIR/SF-TDDFT method, starting from the ground state equilibrium structure of each molecule. The BHHLYP functional[39,40] and the 6-31G* basis set were employed in the SF-TDDFT calculations (indicated by SF-BHHLYP). The reference triplet ground state was calculated based on the spin-restricted open-shell framework. To apply the SMF/SC-AFIR/SF-TDDFT method to relatively large systems, coarse DFT/TDDFT grids were adopted in the initial automated structural search; all obtained MECI structures were then re-optimized using the default DFT/TDDFT parameters in the GAMESS program package.[41] The collision energy parameter for the SC-AFIR method was set to 100 kJ $mol^{-1}$, a value that was confirmed as appropriate in our previous study.[26] The $S_1$-minimum geometry near the FC-point was optimized from the FC-point. The TS geometries between $S_{1\,MIN}$ and the MECIs were optimized for each PAH. For the $S_{1\,MIN}$ and TS geometries, the Gibbs free energies in the gas phase were computed at 298.15 K and 1.0 atm. For comparison, the three most stable MECIs of benzene were further optimized using MS-CASPT2/cc-pVDZ calculations for the lowest two singlet states, where the six electrons in six orbitals active space was adopted (see the ESI†). All of the SF-TDDFT calculations were performed using the GAMESS program,[41] and the CASPT2 calculations were performed using the Molpro2012 program.[42] The structural deformations and optimizations under the SMF/SC-AFIR approach were performed using a developmental version of the GRRM program.[43]

## Acknowledgements

This work was partly supported by a grant from the Japan Science and Technology Agency with a Core Research for Evolutional Science and Technology (CREST) in the Area of ''Establishment of Molecular Technology towards the Creation of New Functions'' at Hokkaido University. Some of the calculations were performed at the Research Center for Computational Science, Okazaki, Japan.

## Notes and references

1 F. Bernardi, M. Olivucci and M. A. Robb, *Chem. Soc. Rev.*, 1996, **25**, 321–328.
2 D. R. Yarkony, *Rev. Mod. Phys.*, 1996, **68**, 985–1013.

3 D. R. Yarkony, *Acc. Chem. Res.*, 1998, **31**, 511–518.
4 A. L. Sobolewski, W. Domcke, C. Dedonder-Lardeux and C. Jouvet, *Phys. Chem. Chem. Phys.*, 2002, **4**, 1093–1100.
5 B. G. Levine and T. J. Martinez, *Annu. Rev. Phys. Chem.*, 2007, **58**, 613–634.
6 S. Nanbu, T. Ishida and H. Nakamura, *Chem. Sci.*, 2010, **1**, 663–674.
7 T. Horio, T. Fuji, Y.-I. Suzuki and T. Suzuki, *J. Am. Chem. Soc.*, 2009, **131**, 10392–10393.
8 J. S. Lim and S. K. Kim, *Nat. Chem.*, 2010, **2**, 627–632.
9 D. Polli, P. Altoe, O. Weingart, K. M. Spillane, C. Manzoni, D. Brida, G. Tomasello, G. Orlandi, P. Kukura, R. A. Mathies, M. Garavelli and G. Cerullo, *Nature*, 2010, **467**, 440–445.
10 K. Wang, V. McKoy, P. Hockett and M. S. Schuurman, *Phys. Rev. Lett.*, 2014, **112**, 113007.
11 N. Koga and K. Morokuma, *Chem. Phys. Lett.*, 1985, **119**, 371–374.
12 M. R. Manaa and D. R. Yarkony, *J. Chem. Phys.*, 1993, **99**, 5251–5256.
13 J. M. Anglada and J. M. Bofill, *J. Comput. Chem.*, 1997, **18**, 992–1003.
14 C. Ciminelli, G. Granucci and M. Persico, *Chem. – Eur. J.*, 2004, **10**, 2327–2341.
15 T. W. Keal, A. Koslowski and W. Thiel, *Theor. Chem. Acc.*, 2007, **118**, 837–844.
16 B. G. Levine, J. D. Coe and T. J. Martinez, *J. Phys. Chem. B*, 2008, **112**, 405–413.
17 F. Sicilia, L. Blancafort, M. J. Bearpark and M. A. Robb, *J. Chem. Theory Comput.*, 2008, **4**, 257–266.
18 S. Maeda, K. Ohno and K. Morokuma, *J. Chem. Theory Comput.*, 2010, **6**, 1538–1545.
19 S. Maeda, K. Ohno and K. Morokuma, *J. Phys. Chem. A*, 2009, **113**, 1704–1710.
20 S. Maeda, T. Taketsugu, K. Ohno and K. Morokuma, *J. Am. Chem. Soc.*, 2015, **137**, 3433–3445.
21 Y. H. Shao, M. Head-Gordon and A. I. Krylov, *J. Chem. Phys.*, 2003, **118**, 4807–4818.
22 F. Wang and T. Ziegler, *J. Chem. Phys.*, 2004, **121**, 12191–12196.
23 N. Minezawa and M. S. Gordon, *J. Phys. Chem. A*, 2009, **113**, 12749–12753.
24 S. Maeda, T. Taketsugu and K. Morokuma, *J. Comput. Chem.*, 2014, **35**, 166–173.
25 Y. Harabuchi, S. Maeda, T. Taketsugu, N. Minezawa and K. Morokuma, *J. Chem. Theory Comput.*, 2013, **9**, 4116–4123.
26 S. Maeda, Y. Harabuchi, T. Taketsugu and K. Morokuma, *J. Phys. Chem. A*, 2014, **118**, 12050–12058.
27 K. N. Houk, P. S. Lee and M. Nendel, *J. Org. Chem.*, 2001, **66**, 5517–5521.
28 M. C. dos Santos, *Phys. Rev. B: Condens. Matter Mater. Phys.*, 2006, **74**, 045426.
29 M. Bendikov, H. M. Duong, K. Starkey, K. N. Houk, E. A. Carter and F. Wudl, *J. Am. Chem. Soc.*, 2004, **126**, 7416–7417.
30 J. Hachmann, J. J. Dorando, M. Aviles and G. K. Chan, *J. Chem. Phys.*, 2007, **127**, 134309.
31 H. F. Bettinger, *Pure Appl. Chem.*, 2010, **82**, 905–915.
32 Y.-L. Wang and G.-S. Wu, *Int. J. Quantum Chem.*, 2008, **108**, 430–439.
33 Y. Kurashige and T. Yanai, *Bull. Chem. Soc. Jpn.*, 2014, **87**, 1071–1073.
34 K. Binran, Handbook of Chemistry, in *Pure Chemistry*, Chem. Soc. Jpn., Maruzen, Tokyo, 5th edn, 2004, section 15.8.4.
35 M. J. Bearpark, M. A. Robb and H. B. Schlegel, *Chem. Phys. Lett.*, 1994, **223**, 269–274.
36 Q. Li, D. Mendive-Tapia, M. J. Paterson, A. Migani, M. J. Bearpark, M. A. Robb and L. Blancafort, *Chem. Phys.*, 2010, **377**, 60–65.
37 L. Blancafort and M. A. Robb, *J. Chem. Theory Comput.*, 2012, **8**, 4922–4930.
38 D. G. Truhlar, B. C. Garrett and S. J. Klippenstein, *J. Phys. Chem.*, 1996, **100**, 12771–12800.
39 A. D. Becke, *Phys. Rev. A: At., Mol., Opt. Phys.*, 1988, **38**, 3098–3100.
40 C. T. Lee, W. T. Yang and R. G. Parr, *Phys. Rev. B: Condens. Matter Mater. Phys.*, 1988, **37**, 785–789.
41 M. W. Schmidt, K. K. Baldridge, J. A. Boatz, S. T. Elbert, M. S. Gordon, J. H. Jensen, S. Koseki, N. Matsunaga, K. A. Nguyen, S. J. Su, T. L. Windus, M. Dupuis and J. A. Montgomery, *J. Comput. Chem.*, 1993, **14**, 1347–1363.
42 H.-J. Werner, P. J. Knowles, G. Knizia, F. R. Manby, M. Schutz, P. Celani, T. Korona, R. Lindh, A. Mitrushenkov, G. Rauhut, K. R. Shamasundar, T. B. Adler, R. D. Amos, A. Bernhardsson, A. Berning, D. L. Cooper, M. J. O. Deegan, A. J. Dobbyn, F. Eckert, E. Goll, C. Hampel, A. Hesselmann, G. Hetzer, T. Hrenar, G. Jansen, C. Koppl, Y. Liu, A. W. Lloyd, R. A. Mata, A. J. May, S. J. McNicholas, W. Meyer, M. E. Mura, A. Nicklass, D. P. O'Neill, P. Palmieri, D. Peng, K. Pfluger, R. Pitzer, M. Reiher, T. Shiozaki, H. Stoll, A. J. Stone, R. Tarroni, T. Thorsteinsson and M. Wang, *MOLPRO, version 2012.1, a package of ab initio* programs, see http://www.molpro.net, accessed May 18, 2015.
43 S. Maeda, Y. Osada, Y. Harabuchi, T. Taketsugu, K. Morokuma and K. Ohno, *GRRM, a developmental version*, Hokkaido University, Sapporo, 2015.